POLITECNICO DI TORINO
Repository ISTITUZIONALE

The Potential of Cations for Carbon Dioxide Electroreduction

Original
The Potential of Cations for Carbon Dioxide Electroreduction / Dattila, F., López, N.. - In: CHEMCATCHEM. - ISSN 1867-3899. - 17:20(2025). [10.1002/cctc.202500749]

Availability:
This version is available at: 11583/3004260 since: 2025-10-20T13:09:35Z

Publisher:
John Wiley and Sons

Published
DOI:10.1002/cctc.202500749

Terms of use:

This article is made available under terms and conditions as specified in the corresponding bibliographic description in the repository

Publisher copyright

(Article begins on next page)

16 November 2026

Check for updates

ChemCatChem

Perspective
doi.org/10.1002/cctc.202500749

Chemistry Europe
European Chemical Societies Publishing

www.chemcatchem.org

The Potential of Cations for Carbon Dioxide Electroreduction

Federico Dattila*[a] and Núria López[b]

The electrochemical reduction of carbon dioxide (eCO_2R) allows both the reduction of anthropogenic greenhouse gas emissions and the storage of intermittent renewable energy. While modeling studies have focused on the catalyst for at least two decades, recently the electrolyte–electrode interface has attracted significant attention, especially metal cations. In this Perspective, we propose simple rules to predict the extent of cation effects on eCO_2R and water reduction depending on the transition metal catalyst, which we later extend to the case of alkali cation-induced surface dissolution. First, we highlight the difficulty of activating CO_2 and the crucial boost that cations provide for late transition metals. Then we re-interpret state-of-the-art results in terms of a unique descriptor, *i.e.*, cation-induced electrostatic potential. Finally, we suggest a possible qualitative explanation for cation effects in cathodic dissolution and mention strategies to overcome cation-induced salt formation. The final Outlook lists directions that the modeling field should follow, *i.e.*, either simplicity (Computational Cation Electrode) or complexity (Multiscale models), showing the potential of simulations toward the understanding of novel electrochemical processes (*i.e.*, eCO_2R in organic cations).

1. Introduction

The possibility of converting carbon dioxide, water, and electricity into useful products, the so-called electrochemical reduction of carbon dioxide (eCO_2 R), is well known for more than 70 years.[1,2] Hori and co-workers provided a crucial boost in this research field in the 1980s, tackling important aspects of this process that are still relevant today. Among them, we here acknowledge the observation of multicarbon products on Cu,[3,4] the classification of eCO_2R selectivity trends depending on Cu structure sensitivity[5] and transition metals,[6] the identification of adsorbed CO as a crucial intermediate,[7,8] report of eCO_2R activity on Ni,[9] eCO_2R activity in organic electrolyte,[10] surface deactivation effects,[11] and ultimately electrolyte cation effects.[12]

As a proof of Hori's impact on eCO_2R, several relevant theoretical and experimental follow-ups originated from the above-mentioned concepts. Rationalizing results in Ref. [6], Bagger et al. identified four main eCO_2R selectivity groups within transition metals: i) strong *CO binding elements prone to CO poisoning (e.g., Ni, Fe, Pt, Pd); ii) weak *CO binding catalysts, selective to CO (e.g., Au, Ag, Cu); iii) weak *H and *CO binding elements selective to formic acid/formate (e.g., Sn, In, Bi); and iv) Cu, with mild *CO binding strength and thermoneutral hydrogen adsorption, which adsorbs CO strongly enough to enable coupling, yet not so strongly as to determine poisoning.[13] In a follow-up study, again Bagger and co-workers carried out a principal component analysis (PCA) study on Hori's eCO_2R study on Cu facets,[5] identifying Cu domains responsible for methane, acetaldehyde, ethylene, and ethanol.[14] Following Hori's hypothesis, many spectroscopic and theoretical works have focused on the role of *CO to open the pathway to multicarbon products, as for instance the first observation of hydrogenated CO–CO dimer by Koper and co-workers.[15] It took almost 30 years of research to upgrade Hori's report of eCO_2R activity on Ni,[9] as only in 2022 Yeo and co-workers demonstrated that inorganic nickel oxygenate-derived catalysts convert carbon dioxide to C_3–C_6 hydrocarbons with 6.5% Faradaic efficiency.[16] Later, analogous activity was found on nickel at high pressure and temperature,[17] and further mechanistic insights were inferred on F-doped Ni.[18] Regarding Hori's observation of Cu deactivation,[11] recently a plethora of studies have confirmed cathodic corrosion[19–21] and surface dissolution[22–27] under eCO_2R conditions.

While many of Hori's contributions have been scrutinized in the last decade, one of the observation, *i.e.*, the dependence of CO_2/CO reduction activity on cationic species,[12] has been left until recent years. Although that Cs^+ outperforms K^+ for CO_2 reduction is a common knowledge, experimentalists still resort to use $KHCO_3$, primarily as a matter of cost reduction and standardization. Three main theories were proposed to rationalize cation effects. In short, besides i) Hori's hypothesis, *i.e.*, modification of the local electric field,[12,28] cations were proposed to ii) buffer the interfacial pH,[29–31] and iii) stabilize crucial intermediates *via* short-term electrostatic interactions.[32,33] These theories are nicely summarized in two review articles by Waegaele et al. (from a more experimental perspective)[34] and Ringe (with a theoretical point of view and focus on hydro-

[a] Dr. F. Dattila
CREST Group, Department of Applied Science and Technology (DISAT), Politecnico di Torino, Corso Duca degli Abruzzi 24, Turin 10129, Italy
E-mail: federico.dattila@polito.it

[b] Prof. N. López
Institute of Chemical Research of Catalonia (ICIQ-CERCA), The Barcelona Institute of Science and Technology (BIST), Avinguda dels Països Catalans 16, Tarragona 43007, Spain

Supporting information for this article is available on the WWW under https://doi.org/10.1002/cctc.202500749

© 2025 The Author(s). ChemCatChem published by Wiley-VCH GmbH. This is an open access article under the terms of the Creative Commons Attribution License, which permits use, distribution and reproduction in any medium, provided the original work is properly cited.

© 2025 The Author(s). ChemCatChem published by Wiley-VCH GmbH

18673899, 2025, 20, Downloaded from https://chemistry-europe.onlinelibrary.wiley.com/doi/10.1002/cctc.202500749 by Politecnico Di Torino Sist. Bibl Del Polit Di Torino, Wiley Online Library on [20/10/2025]. See the Terms and Conditions (https://onlinelibrary.wiley.com/terms-and-conditions) on Wiley Online Library for rules of use; OA articles are governed by the applicable Creative Commons License

gen evolution)[35] and it is beyond the scope of the current publication to discuss them.

Herein, we aim to provide a clear perspective on very recent findings on cation effects in electrochemical CO_2 reduction,[36,37] hydrogen evolution,[38,39] and surface dissolution.[26,27] Inspired by the classification work on cation effects on single atom catalysts[40] and report of eCO_2R on $Pd_{ML}Pt(111)$ even without cations,[41] we first differentiate between "cation-assisted" catalysts (Au, Ag, Cu)[36] and "cation-independent" catalysts (Co, Fe, Ni, Pd, Ru, Rh, Pt, Ir) at mild overpotentials, explaining their different in terms of *d*-band center ϵ_d. Secondly, building on the concept of cation-coupled electron transfer (CCET) reactions introduced by Koper in eCO_2R,[42] we re-interpret previous trends of cation accumulation driving force, CO_2 adsorption energy, and water dissociation activation energy in terms of cation-induced localized electrostatic potential $\phi^{M^{n+}}$. Lately, we reconcile recent observations of cation-induced surface dissolution[26,27,43] with the theory of cathodic corrosion,[20] identifying promotional and inhibitory effects of alkali cations based on the state-of-the-art. Regarding the detrimental phenomenon of cation-induced salt formation during eCO_2R, we list strategies to overcome this limitation.[44–48] In the final Outlook, we discuss future directions in modeling cation effects and a promising field of study.

2. The Carbon Dioxide Reduction Problem

The first challenge experienced by any first-year Ph.D. student applying density functional theory (DFT) to eCO_2R is CO_2 activation. In fact, CO_2 is not stable on the surface of common eCO_2R catalysts, such as Cu, Ag, Au, unless cations or excess charges are present.[49] This simple evidence matches very well with experimental observation.[36] Nevertheless, given the lack of alternative approaches and the comfort of using the computational hydrogen electrode (CHE) framework,[50] the computational community has very often considered CO_2R to COOH as a proton-coupled electron transfer step.[51] Experimental results, instead, point toward a simple electron transfer step on late transition metals,[52] although the equilibrium potential required to form a CO_2^{*-} is rather negative (–1.90 V vs. SHE),[53] if compared to standard onset potential for eCO_2R. Since an activated CO_2 molecule is bent, a rough guess of the energy cost to activate CO_2 is the energy variation from moving the activation angle α from 180 to 120 degrees.[54] Without any electron transfer, more than 3 eV is required for this step, while this thermodynamic cost is lowered to 1 eV, provided that 1 electron transfer takes place (Figure 1a). Given the thermoneutral *H binding energy of many transition metals[13] and the significantly higher concentration of water (55.500 M) rather than carbon dioxide (0.033 M) in aqueous-based electrolyte, the challenge of converting carbon dioxide at high reaction rates comes as a logical consequence.

From a molecular perspective, the hurdle to activate CO_2 can be easily visualized by comparing the density of states within the *d*-band of Au(111) $p(3 \times 3)$ and the CO_2 adsorbate (with frozen geometry to ensure stability), see Figure 1b. The carbon dioxide Lowest Unoccupied Molecular Orbital (LUMO) lies right above gold *d*-band center, preventing the electron transfer from the surface to the adsorbate. If a cation is present, however, the LUMO of the adsorbate is downshifted due to the cation-induced electric field (Figure 1c), ensuring the formation of negatively charged intermediates both from CO_2 activation and CO–CO coupling.[37] In line with this scheme, we thus expect metals with shallow *d*-band states to be able to activate CO_2 even without a metal cation close-by. In line with this hypothesis, in fact, Ye *et al.* observed CO_2 reduction activity to CO and formate on $Pd_{ML}Pt(111)$ even in absence of metal cation in solution.[41]

For the sake of generalization, we resolved to DFT. We employed the Perdew-Burke-Ernzerhof (PBE) density functional,[56] accounting for van der Waals interactions through the DFT-D2 method.[57,58] C_6 coefficients were retrieved from the parametrization derived by López and co-workers.[59] We represented inner electrons through Projector Augmented Wave (PAW) pseudopotentials[60,61] and the monoelectronic states for the valence electrons were expanded as plane waves with a kinetic energy cutoff of 450 eV. The Brillouin zone was sampled by a Γ-centered *k*-points mesh from the Monkhorst–Pack method,[62] with a reciprocal grid size smaller than 0.03 $Å^{-1}$. The lowest energy facets were considered for the transition metals, *i.e.*, Fe(110), Ru(0001), Co(0001), Rh(111), Ir(111), Ni(111), Pd(111), Pt(111), Cu(111), Ag(111), Au(111) with extension $p(3 \times 3)$.[63] The vacuum between the slabs was larger than 10 Å and dipole correction was included in the simulation to account for artificial contributions from the asymmetric slab model.[64]

We estimated CO_2 adsorption energy following the following standardized protocol: i) ionic optimization of *COOH adsorbed *via* terminal oxygen and carbon; ii) removal of hydrogen; iii) ionic optimization of resulting $*CO_2$ geometry; iv) if CO_2 desorbs, we repeat the previous step by carrying out a single point simulation on the frozen $*CO_2$ geometry.

CO_2 ionic optimization proved successful on any transition metal surface apart from Au(111), Ag(111), and Cu(111). A clear trend of ΔE_{*CO_2} vs. *d*-band center of the metal arises (Figure 2a), confirming that elements with shallow *d*-band states can stabilize $*CO_2$ even in absence of metal cations, while Au, Ag, Cu do need a cation, in line with Ref. [36]. Out of these results, transition metals can be classified between "cation-independent" (green elements in Figure 2b) and "cation-assisted" elements (red elements in Figure 2b).

Increased surface charge density σ and applied electric field $\vec{E}$ determine a systematic up-shift of the *d*-band center of the transition metals up to +1.5 eV at $\sigma \sim -0.9$ C/m^2 and up to +0.22 eV at $\vec{E} = -0.6$ V/Å (see Figure 2c), based on data in Figures S1 and S2 and Tables S1 and S2). Therefore, provided enough electric field and surface electronic density, Cu, Ag, and Au could transition from the "cation-assisted" to the "cation-independent" group, suggesting that at high enough overpotentials eCO_2R occurs on late transition metals even without alkali cations. In line with such prediction, El-Nagar *et al.* reported eCO_2R activity on Cu-based zero-gap membrane electrode assembly even in absence of alkali cations in the anolyte.[65] Nevertheless, we note that such observation may also be due to the presence of alkali cations impurities in aqueous media.

© 2025 The Author(s). ChemCatChem published by Wiley-VCH GmbH

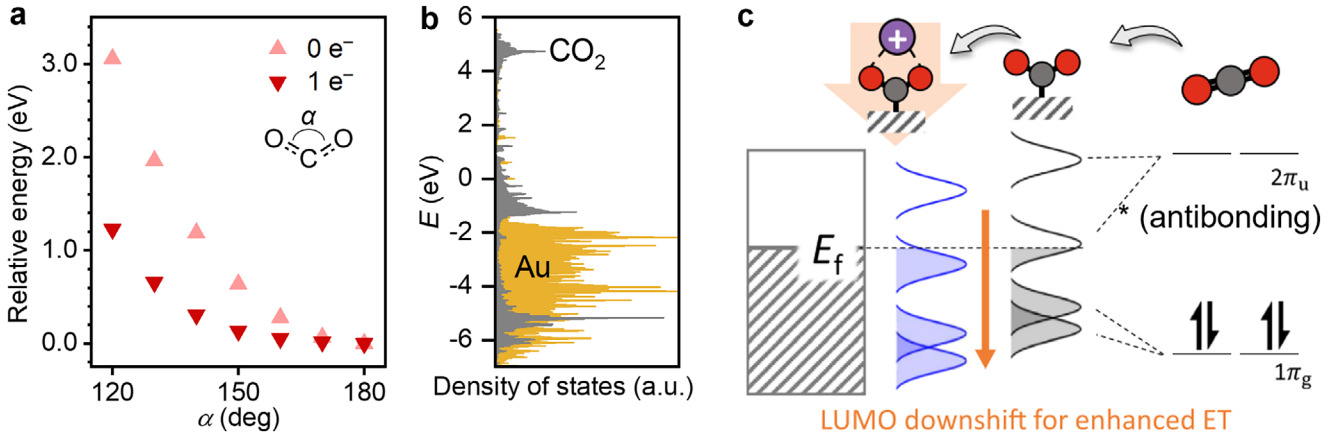


Figure 1. a) Estimated energy for CO_2 activation with (dark red downward triangles) and without (light red upward triangles) additional electrons on the molecule. b) Density of states for Au(111) 3×3 supercell (gold, *d*-band) and CO_2 (gray, *s*- and *p*-bands). c) Downshift of carbon dioxide lowest unoccupied molecular orbital (LUMO) if coupled to a neighboring cation. In grey the Fermi energy the metallic surface is given. Panel (a) reproduced with permission.[54] Copyright 2018 American Chemical Society. Panel (c) reproduced with permission.[37] (Copyright 2022 Springer Nature under Creative Commons Attribution 4.0 International License).[55]

3. Cation-Coupled Electron Transfer Reactions

In this section, first we review the concept of CCET reactions, in line with Koper's formalism, and then we revisit earlier findings in terms of cation-induced electric potential.

3.1. Theory

The concept of CCET was recently applied by Koper[42] and Shin et al.[37] to explain electrocatalytic reaction steps requiring specific cation–adsorbate interactions.[36,38] Although the CCET has had a profound impact on the electrochemical community, it is a well-known phenomenon in organometallics.[66,67] In short, in line with the standard notation employed for bond breaking electron transfer,[42,68] let us consider a model reaction defined as Equation (1), where M^{n+} is a metal cation and $R-X$ is a generic organic molecule which involves an halide bond or in which a bond breaking occurs due to an electron transfer to the lowest unoccupied antibonding molecular orbital (e.g., H_2O dissociation and CO_2 activation). In the presence of a CCET, the Hamiltoniam of the system includes an additional term H_{int}, defined as Equation (2), which represents the interaction between the charge transferred to the molecule and the charge q of the cation. In Equation (2), x is the distance between the reactant (e.g., H_2O or CO_2) and the cation and ϵ_r is the relative dielectric permittivity of the medium (lower than 78.4 within the electrical double layer).[69,70] Taking x as the distance of closest approach, the interactive term in the Hamiltonian represents the cation-induced electrostatic potential, Equation (3). Assuming the strength of the electronic coupling between the antibonding orbital and the metal electronic states to be close to zero,[42] at the equilibrium the activation energy for the cation-coupled electron transfer step is given by Equation (4), which differs from the standard value for non–cation-coupled electron transfers by a factor $\left(1-\frac{\phi_{M^{n+}}}{\lambda+D}\right)$. In Equation (4), λ is the solvent reorganization energy and D the bond dissociation energy.

$$R-X+e^-+M^{n+} \longrightarrow R^{\cdot}+X^-\cdots M^{n+} \tag{1}$$

$$H_{int} \sim \frac{q}{\epsilon_r \cdot x} \tag{2}$$

$$\phi_{M^{n+}} \sim \frac{q}{\epsilon_s \cdot x_0} \tag{3}$$

$$\Delta G(\eta=0)=\frac{\lambda+D}{4}\left(1-\frac{\phi_{M^{n+}}}{\lambda+D}\right) \tag{4}$$

To better exemplify the dependence of CCET rate and cation, Koper then introduces an empirical expression for the case study of the rate-determining Volmer step of hydrogen evolution reaction, in line with Ref. [71]. Assuming for simplicity a nonquadratic dependence between activation energy and cation-induced potential and using the Butler–Volmer expression, water activation reaction rate depends directly on cation surface concentration $[M^{n+}]_{surf}$ and this dependence is mediated by the empirical reaction order γ, see Equation (5).[71] In Equation (5), k_0 is the standard rate constant, α is the charge transfer coefficient, F is the Faradaic constant, E is the applied potential, E_0 the standard potential of water reduction, R the universal gas constant, T the temperature in K. Although this rate definition neglects any pH or mass transfer dependence, both aspects should be considered as they influence surface cation concentration. In fact, typical CCET reactions imply the generation of OH^- at the surface and, since local electroneutrality should be satisfied, a simple direct relationship between OH^- and cation surface concentrations can be determined, see Equation (6), mediated by the local transference number β. Again, this relationship could be investigated in more detail by means of multiphysics modeling.

$$k=k_0\cdot\exp\left(\frac{-\alpha F(E-E_0)}{RT}\right)[M^{n+}]^{\gamma}_{surf} \tag{5}$$

© 2025 The Author(s). ChemCatChem published by Wiley-VCH GmbH

18673899, 2025, 20, Downloaded from https://chemistry-europe.onlinelibrary.wiley.com/doi/10.1002/cctc.202500749 by Politecnico Di Torino Sist. Bibl Del Polit Di Torino, Wiley Online Library on [20/10/2025]. See the Terms and Conditions (https://onlinelibrary.wiley.com/terms-and-conditions) on Wiley Online Library for rules of use; OA articles are governed by the applicable Creative Commons License

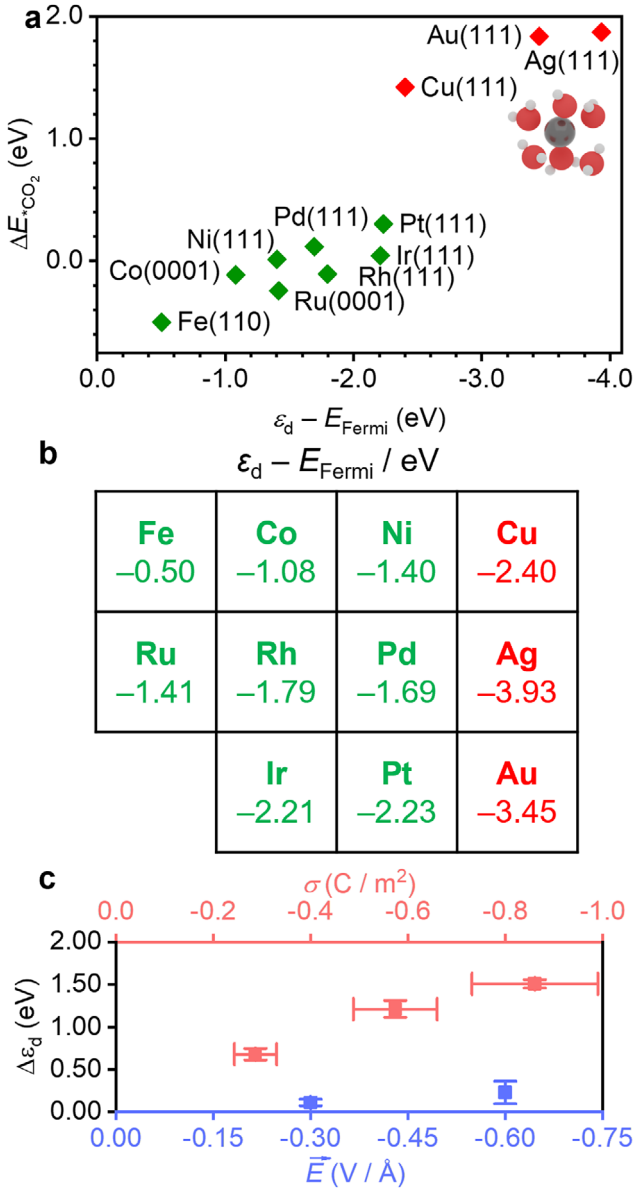


Figure 2. a) Linear scaling relationship between $*CO_2$ adsorption energy and *d*-band center of selected transition metals. For Cu, Ag, Au, single point simulations were performed, as $*CO_2$ is not stable. b) Classification of transition metals based on their *d*-band center. Metals with deep *d*-state require a cation to activate CO_2 (in red),[36] while all other metals can enable CO_2 reduction even without metal cations (in green). c) Up-shift of *d*-band center due to surface charging (light red data points) and electric field within the electrical double layer (light blue data points). Data taken from Tables S1 and S2.

$$[M^{n+}]_{surf} \sim [M^{n+}]_{bulk} + \beta([OH^-_{surf}] - [OH^-_{bulk}]) \quad (6)$$

3.2. Cation Accumulation

The dependence of CCET rates on cation concentration at the surface, Equation (5), has been rationalized and demonstrated by a wide number of studies.[12,28,33,36,38] Thus, cation accumulation at the surface has been modeled using several descriptors: degree of specific adsorption,[12] hydration energy,[54] cation hydrated radius,[28] ionic radius,[36] cation acidity (*i.e.*, ratio of the square of the cation charge divided by the ionic radius).[38] In line with Koper's formalism,[42] we here aim to reexamine these findings in terms of a unique descriptor, cation-induced electrostatic potential $\phi_{M^{n+}}$, which can be easily determined from experimental values,[34,72,73] see Table S3. A more refined investigation on cation mass transfer effects requires multiphysics modeling, as done by Ringe et al.[28] and Lorenzutti et al.[74] which has the drawback, however, of needing *ad hoc* simulations.

Table 1. Reduction potentials for alkali cations. Taken from Ref. [73].

	Li^+	Na^+	K^+	Cs^+
U_0 (V vs SHE)	−3.04	−2.71	−2.93	−3.03

From a computational point of view, a simple thermodynamic parameter to determine the ease for cations to accumulate at the cathode was introduced by Resasco *et al.*[33] In short, the energy of cation/electron pair in the bulk electrolyte $E_{M^+ + e^-,bulk}$ can be derived from the energy of the metal by applying the computational hydrogen electrode (CHE)[50] formalism to cation reduction (Equation 7). In fact, at the equilibrium potential for cation reduction U_0 (Table 1), the process is in equilibrium and the energies of products and reactants are equivalent. Thus, the energy of cation/electron pair in the bulk electrolyte at any applied potential can be estimated from Equation (7).

In turn, the energy of the cation/electron pair at the outer Helmotz plane $E_{M^+ + e^-,OHP}$ can be estimated from DFT simulations. As a final consequence, the energy gained by cations upon accumulating at the surface is given by Equation (9). Taking the partial derivative of this energy gain with respect to the cation-surface distance $d_{M^{n+}-surf}$, the thermodynamic driving force for cation accumulation can be derived.[38]

$$M^+ + e^- \leftrightarrow M, U = U_0 \quad (7)$$

$$E_{M^+e^-,bulk} = E_M - |e^-|(U - U_0) \quad (8)$$

$$\Delta E_{M^+,OHP} = E_{M^+ + e^-,OHP} - E_{M^+ + e^-,bulk} \quad (9)$$

$$\vec{F}_{el} = \frac{\partial(\Delta E_{M^+,OHP})}{\partial(d_{M^+-surf})} \quad (10)$$

In Ref. [36] the energy of a cation-electron couple at the outer Helmholtz plane was estimated for alkali cations by taking the lowest energy configuration during the last 2 ps of *ab initio* molecular dynamics (1 ps equilibration, 5 ps production at 1 fs time step, retrieved from previously optimized water/metal interfaces at 300 K)[75] on $(3\sqrt{3} \times 3\sqrt{3})R30^\circ$ Au(111) (four layers, two outermost layers relaxed, bulk fixed, 1 single cation in the simulation cell).[76] A linear correlation between $\Delta E_{M^+,OHP}$ and cation ionic radius was found,[36] and it was explained in terms of the cation solvation shell: shorter the ionic radius, harder the solvation shell, larger the hydrated radius and lower the accumulation at the surface, following the trend $Li^+ < Na^+ < K^+ < Cs^+$. In Ref. [38] the driving force for cations to accumulate at the surface was estimated by fitting cation/electron pair energy vs cation-surface

© 2025 The Author(s). ChemCatChem published by Wiley-VCH GmbH

18673899, 2025, 20, Downloaded from https://chemistry-europe.onlinelibrary.wiley.com/doi/10.1002/cctc.202500749 by Politecnico Di Torino Sist. Bibl Del Polit Di Torino, Wiley Online Library on [20/10/2025]. See the Terms and Conditions (https://onlinelibrary.wiley.com/terms-and-conditions) on Wiley Online Library for rules of use; OA articles are governed by the applicable Creative Commons License

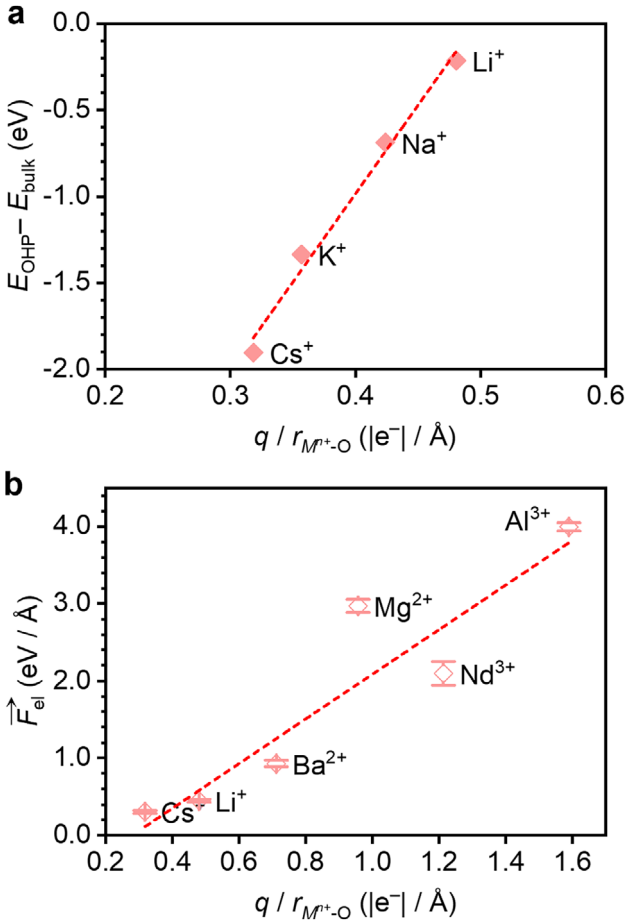


Figure 3. Dependence of a), energy gain by moving cations from bulk electrolyte to the outer Helmholtz plane and b), thermodynamic driving force for cation repulsion on cation-induced electrostatic potential for a water/Au(111) supercell. Data points were retrieved from Refs. [36, 38].

distance over 50 snapshots of the *ab initio* molecular dynamics trajectory taken every 20 fs (after 1 ps equilibration, analogous methodology as in Ref. [36], 2 cations in the simulation cell).[77] Such electrostatic accumulation force was then plotted vs cation acidity, confirming a linear correlation.[38] This observation was explained in terms of cation repulsion: higher the cation acidity, more repulsion between neighboring cations, lower the accumulation at the surface, following the acidity trend $Cs^+ < Li^+ < Ba^{2+} < Mg^{2+} < Nd^{3+} < Al^{3+}$. We here demonstrate that both these properties, energy gain for cation accumulation $\Delta E_{M^+,OHP}$ and $\vec{F}_{el}$ driving force, linearly correlate with the cation-induced electrostatic potential (Figure 3a,b), derived in line with Koper's formalism as Equation (3) and given in units of | e⁻| /Å (see Table S3), see Equation (11) ($r^2 = 0.987$, $\chi^2 = 0.02$) and Equation (12) ($r^2 = 0.90$, $\chi^2 = 387.52$). The physical implication of these linear correlations is twofold: lower the cation-induced potential, i) softer the solvation shell and ii) lower the repulsion between neighboring cations, leading to more accumulation at the surface according to the trend $Cs^+ > Li^+ > Ba^{2+} > Mg^{2+} > Nd^{3+} > Al^{3+}$.

$$\Delta E_{M^+,OHP} = -(5.1 \pm 0.3) + (10.2 \pm 0.8) \cdot \phi_{M^+} \quad (11)$$

$$\vec{F}_{el} = (0.8 \pm 0.2) + (2.9 \pm 0.4) \cdot \phi_{M^{n+}} \quad (12)$$

3.3. CO_2 Activation

As previously discussed, the concept of CCET applies directly to the CO_2 activation step. Experimentally, it has been demonstrated that CO_2 electroreduction does not occur in aqueous media on Cu, Ag, Au unless a metal cation is present,[36] while we have observed in Figure 2 that metals with deep *d*—band states can activate carbon dioxide even without cations. Under the mean-field hypothesis introduced originally by Hori and co-workers and retrieved by Ringe *et al.*,[12,28] cations induce a modulation of electric field within the electrical double layer. This modulated electric field has then a direct influence on the adsorption energy of a given intermediate depending on its electric dipole moment $\vec{p}$ and polarizability α.[32,33]

Chen et al. directly tested this hypothesis.[32] By inserting solvated cations close to the surface (K^+ and 1-ethyl-3-methylimidazolium, $EMIM^+$), they observed the appearance of a very localized electric field of the order of −1.0 V/Å^1, which decays beyond a radial distance of 5 Å. The electric field at a given radial distance $\vec{r}$ from the cation was derived from the resulting variation of electrostatic potential due to charged species, Equation (13), where surf, solv, and cat stand for surface, solvent molecules, and cation respectively. Hence, the cation-induced electric field, $\vec{E}_{cat}$, is given by Equation (14), where $\vec{r}_{ads}$ and $\vec{r}_{cat}$ are the coordinates of adsorbate and alkali cation. The additional negative sign highlights that the electric field is estimated for a negative unit charge. By estimating CO_2 adsorption energy versus the applied electric field $\vec{E}$, induced by an external dipole potential under vacuum,[78] the authors eventually proved that cation stabilization is analogous to a mean-field effect mediated by intermediate dipole moment $\vec{p}$, polarizability α, and mean electric field $\vec{E}$ (Equation 15):

$$U(\vec{r}) = U_{surf/solv/cat} - U_{surf} - U_{solv} - U_{cat} \quad (13)$$

$$-\vec{E}_{cat} = -\left(-\frac{U(\vec{r}_{ads}) - U(\vec{r}_{cat})}{\|\vec{r}_{ads} - \vec{r}_{cat}\|}\right)\hat{r} \quad (14)$$

$$E(\vec{E}) = E(\vec{E} = 0\text{VÅ}^{-1}) + \vec{p} \cdot \vec{E} - \frac{\alpha|\vec{E}|^2}{2} \quad (15)$$

This approach has been used until recent years, neglecting any relevant short-term interaction between cation and adsorbates.[28,32,33] It is, however, not ideal for generalizing cation effects to different reaction intermediates and alkali cations. In fact, estimation of the mean-field electric field generated by cations requires *ad hoc* density functional theory-based *ab initio* molecular dynamics simulations of metal/water interface,[36,38,75] or multiphysics modeling.[28,74,79] Besides, in Ref. [36] we put forward the relevance of specific electrostatic interactions between cation and carbon dioxide. Specifically, we introduced the concept of cation–carbon dioxide coordination number $N_{M^{n+}-O}$, revealing that this observable correlates directly with CO_2 activation ability, *i.e.*, the larger the coordination number, the higher

© 2025 The Author(s). ChemCatChem published by Wiley-VCH GmbH

18673899, 2025, 20, Downloaded from https://chemistry-europe.onlinelibrary.wiley.com/doi/10.1002/cctc.202500749 by Politecnico Di Torino Sist. Bibl Del Polit Di Torino, Wiley Online Library on [20/10/2025]. See the Terms and Conditions (https://onlinelibrary.wiley.com/terms-and-conditions) on Wiley Online Library for rules of use; OA articles are governed by the applicable Creative Commons License

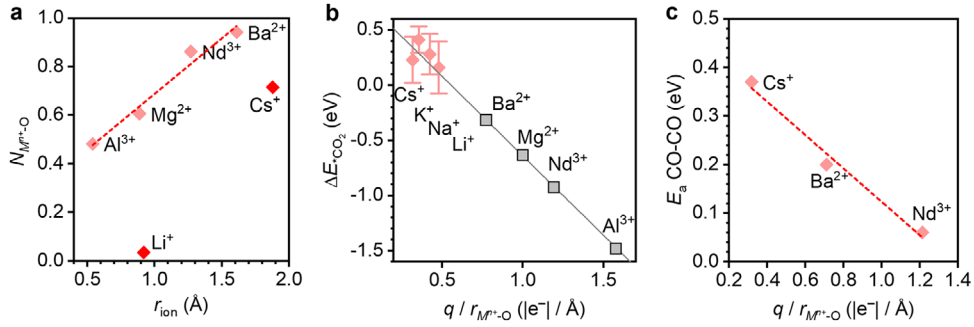


Figure 4. a) Dependence of coordination number between multivalent cation M^{n+} and terminal oxygen of adsorbed carbon dioxide vs cation ionic radius derived for a water/Au(111) supercell. b) Correlation of $*CO_2$ adsorption energy (light red data points) vs cation-induced electrostatic potential on a water/Au(111) supercell. Predicted cation-induced stabilization is reported as solid black line, with extrapolated $*CO_2$ adsorption energy for multivalent cations. c) Correlation of activation energy for CO–CO coupling vs cation-induced potential on Cu(100) with 1 cation and three explicit solvent molecules. Data points in Panels (a) and (b) were retrieved from Ref. [38].

the CO_2 reduction reaction rate. The mechanistic picture is the following. Cation stabilization is first of all mediated by the rate of interaction, quantified by $N_{M^{n+}\text{-O}}$. Once cation and adsorbate interact, the extent of this stabilization is quantified in around 0.5 eV for each alkali cation.[36] By the time we could not derive any explanation for such value. Again, the use of $N_{M^{n+}\text{-O}}$ descriptor has limitations, as its estimation requires lengthy *ab initio* molecular dynamics simulations on metal–water interface with explicit metal cations.[36,38]

Here, we demonstrated that both cation–CO_2 coordination number and the extent of stabilization can be derived out of cation properties (see Table S3).[34,72,73] Starting from $N_{M^{n+}\text{-O}}$, a careful analysis suggests that, for a given cation valency (+1, +2, +3), a linear correlation between cation–CO_2 coordination number and cation ionic radius occurs, see Figure 4a. While alkali cations show a different dependence as bi- and tri-valent ones, a well-defined linear trend is derived for multivalent cations, see Equation (16) ($r^2 = 0.95$, $\chi^2 = 4.2 \cdot 10^{-3}$). Thus, the rate of cation–CO_2 interaction can be directly determined from the cation ionic radii.[73] In turn, the extent of stabilization induced by each cation can be quantified depending on cation-induced electrostatic potential, estimated from cation charge and oxygen-cation distance in line with Koper's notation.[42] In simple electrostatic terms, we expect cation to decrease the Gibbs free energy of adsorption of CO_2 by a potential energy term mediated by cation–carbon dioxide distance ($d_{M^{n+}\text{-O}}$), cation and adsorbate charges (q_{int}, $q_{M^{n+}}$), and the dielectric permittivity of water at the electric double layer (ϵ_r). By assuming a dielectric permittivity of 10,[69,70] the cation-induced stabilization extrapolated from Equation (17) matches very well the CO_2 adsorption energy computed *via* DFT simulation in Ref. [36]. As a last observation, we note that an analogous linear correlation is observed between CO coupling activation energy and cation-induced potential, see Equation (18) ($r^2 = 0.97$, $\chi^2 = 7.6 \cdot 10^{-4}$) derived from the fitting in Figure 4c. These simulations were carried out specifically with the PBE density functional[56] on Cu(100) $p(3 \times 3)$, with one explicit cation and three explicit solvent molecules.[80]

$$N_{M^{n+}\text{-O}} = (0.23 \pm 0.07) + (0.46 \pm 0.06) \cdot r_{ion} \quad (16)$$

$$\Delta G = \Delta G(\text{no cat}) + \frac{1}{4\pi\epsilon_0\epsilon_r}\frac{q_{int} \cdot q_{M^{n+}}}{d_{M^{n+}\text{-O}}} \quad (17)$$

$$E_a(\text{CO-CO}) = (0.47 \pm 0.04) - (0.34 \pm 0.04) \cdot \phi_{M^{n+}} \quad (18)$$

3.4. H_2O Reduction

The Volmer step in water reduction (H_2OR) is another case of CCET. Cation effects on H_2OR have been observed in many research works (for instance, see Refs. [38, 39, 71, 81–83]) and have been nicely discussed in a review paper by Ringe.[35] In short, in neutral to alkaline electrolytes, reaction rate for water reduction decreases on Ir, Pd, Pt along the alkali cation group ($Cs^+ < K^+ < Na^+ < Li^+$), while it increases on Cu, Ag, Au ($Cs^+ > K^+ > Na^+ > Li^+$).[39,83] This cation dependence is absent in acidic electrolyte,[39] where H^+ is the main proton source.

The cation dependence of water reduction rate has been explained in terms of stabilization of the transition state for water activation.[84] A direct correlation between *OH adsorption energy and water reduction rates was observed on Ru-modified and bare Pt facets,[84] and motivated by a possible linear scaling relationship between ΔE_{*OH} and the energy of the transition state. Building on top of these insights,[84] Bender *et al.* demonstrated *via* DFT a twofold cation effects on water reduction: i) stabilization of the transition state, leading to higher activity on Ag, Au, Cu; ii) stabilization of adsorbed hydroxide, leading to harder removal on Pt, Pd, and Ir and consequent lower water reduction activity.

In Ref. [38] we generalized cation effects on proton, hydronium, and water reduction by showing linear scaling relationships of $\Delta G(*H_3O^+\text{diss})$ and $E_a(H_2O\text{diss})$ with respect to cation acidity, while no dependence on acidity was found for $\Delta G(*H)$. As an additional confirmation of the beauty of the cation-induced potential descriptor, analogous linear scaling relationships can be derived vs $\phi_{M^{n+}}$ (Figure 5). In particular, no correlation is found for *H Gibbs Free energy, see Equation (19) (r^2 =-0.06, $\chi^2 = 2.4 \cdot 10^{-2}$), as expected by Equation (17) assuming a near-zero negative charge on the adsorbate q_{int}. Instead, hydronium dissociation energy and activation energy for water dissociation correlate negatively with cation-induced electro-

© 2025 The Author(s). ChemCatChem published by Wiley-VCH GmbH

18673899, 2025, 20, Downloaded from https://chemistry-europe.onlinelibrary.wiley.com/doi/10.1002/cctc.202500749 by Politecnico Di Torino Sist. Bibl Del Polit Di Torino, Wiley Online Library on [20/10/2025]. See the Terms and Conditions (https://onlinelibrary.wiley.com/terms-and-conditions) on Wiley Online Library for rules of use; OA articles are governed by the applicable Creative Commons License

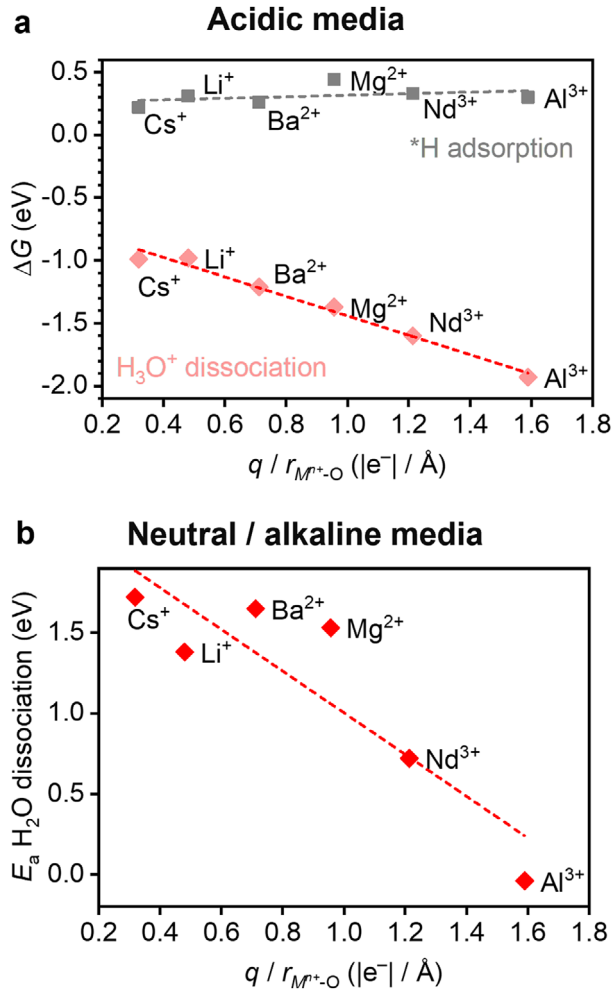


Figure 5. Correlation of a) Gibbs free energy for *H adsorption (gray) and H_3O^+ dissociation (light red) and b) water dissociation activation energy vs cation-induced electric field. Simulations carried out on Au(111) with 1 cation and three explicit water molecules. Data points in Panels (a) and (b) were retrieved from Ref. [38].

static potential, see Equation (20) (r^2 =0.98, $\chi^2 = 1.2 \cdot 10^{-2}$) and Equation (21) ($r^2$ =0.49, $\chi^2 = 7.4 \cdot 10^{-1}$), with slopes of -0.77 ± 0.05 and -1.2 ± 0.3, which, in line with Equation (17), represent the charge acquired by the adsorbate once the transition state is reached.

$$\Delta G(*\mathrm{H}) = (0.26 \pm 0.07) + (0.06 \pm 0.07) \cdot \phi_{M^{n+}} \quad (19)$$

$$\Delta G(*\mathrm{H_3O^+diss}) = -(0.67 \pm 0.05) - (0.77 \pm 0.05) \cdot \phi_{M^{n+}} \quad (20)$$

$$E_a(\mathrm{H_2Odiss}) = +(2.3 \pm 0.3) - (1.2 \pm 0.3) \cdot \phi_{M^{n+}} \quad (21)$$

4. Surface Dissolution

Very recently, the concept of surface dissolution has gained momentum in the field of eCO_2R. From some pioneering observation from Cherenko's and Buonsanti's groups,[22,23,85] the community has now moved to systematic observation of this phenomenon on copper under CO_2 reduction conditions.[24,25] Already back in 1898, Haber observed the formation of "clouds" from cathodically polarized metal,[86,87] which now goes under the general term of Cathodic Corrosion. As nicely summarized by Koper *et al.* in a review article,[20] the proposed mechanism for cathodic corrosion, for instance on platinum, is as follows: i) formation of surface hydrides, ii) dissolution of Pt_xH_y anions potentially aided by neighboring cations, iii) oxidation of the anion complexes, iv) nucleation of the re-deposited metal atoms. *Via* a systematic assessment of dissolution rates on different transition metals, Cherevko and co-workers found two main descriptors for dissolution: i) the cohesive energy of the metal atoms (E_{coh}) and ii) the enthalpy of formation of adsorbed oxygen ($\Delta H_{O,ads}$), see Equation (22). The mechanistic picture behind this observation is logical. Metals with higher cohesive energy have stronger metal–metal bonds, preserving them from dissolution. In turns, metals with strong *O adsorption undergo quick dissolution/redeposition cycles, significantly lowering the migration of solutes to the bulk. In fact, we note that dissolution rates are usually quantified *via* online inductively coupled plasma mass spectrometry (ICP-MS), thus high concentration of solutes in the bulk electrolyte is an indication of high surface dissolution, high migration toward the bulk, and low redeposition.

$$r_{diss} \sim e^{-E_{coh}}, e^{\Delta H_{*O,ads}} \quad (22)$$

In line with Ref. [20], cations have been suggested to play a crucial role in surface dissolution and/or cathodic corrosion as well. In one of the pioneering studies, Koper and co-worker carried out extensive investigation on cathodic corrosion on Pt, Rh, and Au.[19] Changes in the surface morphology depending on cation concentration and species were attributed to specific cation adsorption on step edges,[19] whose onset potential was estimated *via* DFT simulations, following the computational approach devised by Janik and co-workers.[88,89] In a recent follow-up study on platinum, Koper and co-workers observed via high-energy-resolution X-ray absorption near-edge structure (XANES) the fingerprints of platinum hydrides species, proposing the existence of tertiary metal hydride complexes driving dissolution (e.g., Na_2PtH_4, Na_2PtH_6).[21] Very recently, Jaramillo and co-workers put forward alkali cation-induced cathodic corrosion on Cu as well, once a potential threshold is overcome (−0.4 V vs. RHE in 0.1 M $KHCO_3$).[26] The extent of surface reorganization depended on metal cation concentration. Remarkably, no significant reconstruction was observed in this study at −1.05 V vs. RHE in 0.05 M H_2SO_4, suggesting that metal cations may be crucial to initiate the process.

Under pulsed electrolysis in CO_2-saturated 0.1 M $MHCO_3$, dissolution rates of copper were shown to increase moving along the alkali group, *i.e.*, $Li^+ < Na^+ < K^+ < Cs^+$.[27] A tentative explanation was given: strong solvation shell cations induce a light dissolution/redeposition cycle, while weak solvation shell cations boost strongly this phenomenon. Finally, very recently Kim *et al.* quantified the concentration of platinum dissolved in bulk electrolyte after 30 repeated CVs (0.05–1.2 V vs. RHE, ν = 200 mV/s) in presence of different alkali cations in 0.05 *M*OH.[43] A negative correlation between dissolution rate and alkali ionic radius was found, *i.e.*, dissolution decreases following the trend

© 2025 The Author(s). ChemCatChem published by Wiley-VCH GmbH

18673899, 2025, 20, Downloaded from https://chemistry-europe.onlinelibrary.wiley.com/doi/10.1002/cctc.202500749 by Politecnico Di Torino Sist. Bibl Del Polit Di Torino, Wiley Online Library on [20/10/2025]. See the Terms and Conditions (https://onlinelibrary.wiley.com/terms-and-conditions) on Wiley Online Library for rules of use; OA articles are governed by the applicable Creative Commons License

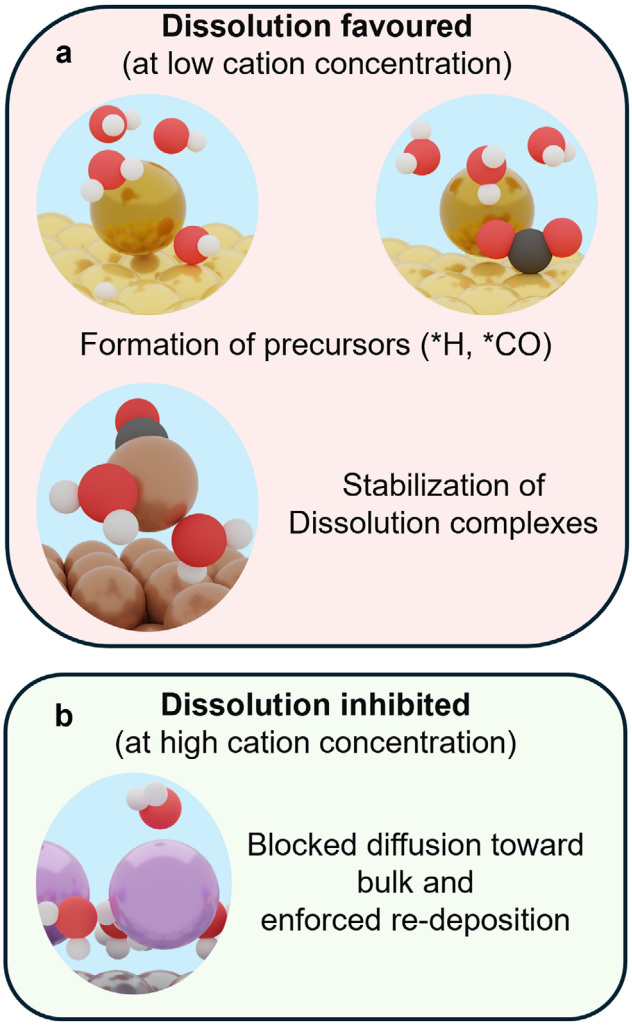


Figure 6. a), Promotional effects on transition metal dissolutions, *i.e.*, evolution of precursors[21,24,25,36,38,39] and stabilization of complexes dissolved in solution.[20] b), Inhibition of complexes migration toward bulk electrolyte due to steric effects and electrostatic repulsion.[43]

$Li^+ > Na^+ > K^+ > Cs^+$. DFT simulations with platinum-explicit water interface highlighted that presence of hydroxides in the supercell ease Pt^{2+} ions diffusion toward the bulk electrolyte by balancing the net charge of the cations and preventing migration toward the surface. This hypothesis was confirmed, as increasing the electrolyte pH from pH 11 to 13 lead to a Pt dissolution increase from ~7 to ~53 ng/cm^{-2}. Consequently, the higher dissolution rate reported in presence of Li^+ was explained in terms of more facile cation hydrolysis, due to its high acidity and low pK_a.[29,38]

Given the previous considerations, we here aim to summarize the hypotheses on positive and negative cation effects on surface dissolution/cathodic corrosion (Figure 6). To benchmark our interpretation, we analyzed experimental entries from 18 state-of-the-art studies on surface reconstruction, dissolution, cathodic corrosion on copper (see Tables S4 and S5). After having properly encoded qualitative entries into numerical values (see Table S6), we carried out a correlation matrix analysis on the variables (Table 2). As discussed earlier, one crucial factor to determine surface dissolution is the cohesive energy of the metal, see Equation (22).

From a purely molecular point of view, metal cohesion can be estimated using the tight-binding model in the second model approximation.[90] The energy per atom of an interacting many-atom system, *i.e.*, a metal facet, depends on its coordination number with neighboring atoms through an attractive term, proportional to the square root of N_{coord}, and a weak repulsive term, which increases linearly with N_{coord}. Thus, lower the coordination number of a surface atom, lower its cohesive energy (see Figure S3).[70] According to Figure S3, evolution is observed on nanoparticles to a larger extent than on single crystal surfaces, because of the overall lower coordination number of surface sites, which decreases the overall energy contained within the system. This is confirmed by a positive correlation between surface evolution and catalyst structure (+0.36, Table 2).

$$E(N_{coord}) = E_0 - A \cdot \sqrt{N_{coord}} + B \cdot N_{coord} \quad (23)$$

Besides, entries with oxidic pretratment also show an higher degree of reconstruction (weak positive correlation, +0.13 in Table 2). Equally, evolution and applied potential exhibit a weak positive correlation (+0.09 in Table 2), more negative the applied potential is, stronger the evolution. Gas species have a significant impact in driving reconstruction as well. To vary the gas feed along the group Air, Ar, N_2, CO_2, CO induce higher rate of evolution (+0.25), in line with the hypothesis of CO-driven Cu dissolution and re-deposition.[24,25] Here we propose the first promoting effect of cations on surface evolution. In line with previous findings,[36,38] metal cations determine high water reduction and CO_2 reduction reaction rates. In turns, this cause the formation of adsorbed hydrides and carbon monoxide species, which can induce metal/surface bond breaking on undercoordinated sites, as proposed in Refs. [20, 21] (for *H$^{\delta-}$) and Refs. [24, 25] (for *CO). The *H-mediated hypothesis is confirmed by the negative correlation between surface evolution and electrolyte species (−0.35 in Table 2). Acidic media with higher surface concentrations of protons lead to higher reconstruction than alkaline media. As a final confirmative note, Raaijman *et al.* reported absence of any reconstruction phenomena on copper at very highly concentrated alkaline media (thus very low proton concentration),[91] provided that initial oxidation was avoided.

A specific interaction between metal cations and relevant dissolution intermediates, either precursors or dissolution complexes, is further validated by a weak positive correlation between cation species M^{n+} and evolution (+0.17 in Table 2), *i.e.*, surface restructuring is eased increasing the alkali cation radius or moving to bi- and tri-valent species,[27] Again, this can be explained in terms of higher formation rates of surface hydrides and carbon monoxide, initiating dissolution, or cation-induced short-term stabilization of dissolution complexes in solution. As a last insight on cation effects, cation concentration exhibits a negative impact on surface evolution (−0.45 in Table 2), *i.e.*, reconstruction decreases at high cation concentration. This can be explained in terms of electrostatic and steric blocking of metal ions diffusion toward the bulk electrolyte and forced re-

© 2025 The Author(s). ChemCatChem published by Wiley-VCH GmbH

18673899, 2025, 20, Downloaded from https://chemistry-europe.onlinelibrary.wiley.com/doi/10.1002/cctc.202500749 by Politecnico Di Torino Sist. Bibl Del Polit Di Torino, Wiley Online Library on [20/10/2025]. See the Terms and Conditions (https://onlinelibrary.wiley.com/terms-and-conditions) on Wiley Online Library for rules of use; OA articles are governed by the applicable Creative Commons License

18673899, 2025, 20, Downloaded from https://chemistry-europe.onlinelibrary.wiley.com/doi/10.1002/cctc.202500749 by Politecnico Di Torino Sist. Bibl Del Polit Di Torino, Wiley Online Library on [20/10/2025]. See the Terms and Conditions (https://onlinelibrary.wiley.com/terms-and-conditions) on Wiley Online Library for rules of use; OA articles are governed by the applicable Creative Commons License

Table 2. Correlation matrix of several variables affecting surface dissolution based on state-of-the-art experimental data encoded (Tables S4 and S5). The label "Oxi" stands for oxidic pretreatment.

	Catalyst	Oxi	*E* (V vs RHE)	Gas	Electrolyte	M^{n+}	*C* (M)	Evolution
Catalyst	1.00	−0.13	+0.17	+0.43	−0.44	+0.16	−0.52	+0.36
Oxi		1.00	+0.14	+0.17	−0.06	−0.08	−0.14	+0.13
E (V vs RHE)			1.00	+0.44	+0.18	+0.28	−0.57	+0.09
Gas				1.00	−0.01	+0.22	−0.51	+0.25
Electrolyte					1.00	+0.01	+0.49	−0.35
M^{n+}						1.00	−0.27	+0.17
C (M)							1.00	−0.45
Evolution								1.00

deposition *via* migration toward the electrode, in line with the very recent findings by Kim et al.[43]

5. pH Buffering and Salt Formation

In addition to phenomena limited to the electrical double layer (stabilization of key intermediates, ionic repulsion) or the diffusion layer (cation accumulation), alkali cations show as well macroscopic effects on the CO_2 reduction performance. According to the charge neutrality principle, in neutral to alkaline pH cations act as the only counterions to negatively charged electrolytes species, *i.e.*, OH^-, CO_3^{2-}, HCO_3^-. Thus, cation flow *J* along the diffusion layer, governed respectively by diffusion, migration, and convection through the Nerst–Planck equation,[92] directly impacts the pH profile. Specifically, cation electromigration depends on its valence *z*, its diffusion coefficient *D* (m^2/s), the electric potential ϕ, and its local concentration *c* (mol/m^3), while the convective term is mediated by the electrolyte velocity $\vec{v}$ (Equation 24). In Equation (24) R, *T*, and F stand, respectively, for the universal gas constant (J/mol · K), the temperature (K), and the Faraday constant (C/mol).

$$\vec{J} = -D\nabla c - \frac{zF}{RT}Dc\nabla\phi + c\vec{v} \tag{24}$$

In addition to influencing OH^- mass transport, according to some recent studies cations also induce pH buffering. To explain cation size trends within Li^+, Na^+, K^+, Rb^+, and Cs^+ during CO_2 reduction tests on Cu and Ag on custom-made gas-tight electrochemical cell at −1.0 V vs RHE, Singh *et al.* developed a 1D mathematical model, specifically accounting for cation hydrolysis.[29,93] Starting from the definition of hydrated cation's pK_a (*i.e.*, the ease for a water molecule within the solvation shell to undergo hydrolysis), the authors estimated cations' pK_a in the bulk electrolyte and close to Cu and Ag cathode at −1.0 V vs. RHE. While cation's pK_a in the bulk increases following the ionic radius, larger ionic radius cations exhibit a lower electrostatic interaction with neighboring water molecules, at the surface weakly hydrated cations (with larger ionic radius) generate higher electrostatic field, leading to larger hydrolysis rates, Table 3.

K^+, Rb^+, and Cs^+, having pK_a at the surface lower than the expected pH,[93] enable hydrolysis, thus leading to release of protons from their solvation shell which buffer pH. Consequently, such buffering prevents neutralization of CO_2 by neighboring OH^-, thus sustaining higher concentrations of CO_2 at the surface. The prediction of higher pH buffering for cations with larger ionic radius was confirmed by a precedent ATR-SEIRAS investigation, probing pH at a gold/electrolyte interface from the CO_2/HCO_3^- bands ratio.[30] A follow-up study estimated CO_2 concentration at a gold electrode from ATR-SEIRAS measurements and demonstrated a negative correlation with cation ionic radius.[94] This observation was explained in terms of higher CO_2 consumption rates due to cation-promoted eCO_2R.

Certainly, the most detrimental effect of cations on CO_2 reduction performance is the formation of salts, which damages the catalytic activity and lowers the carbon conversion efficiency. In fact, given the specific solubility of different electrolytes in water (see Table 4 for K-based salts), local cation and anion con-

Table 3. Estimated pK_a for cations hydrolysis in the bulk electrolyte (bulk) and at the surface layer of copper ($surf_{Cu}$) and silver cathodes ($surf_{Ag}$) at −1.0 V vs. RHE.[29] Taken from Ref. [29].

Cation	Bulk	$Surf_{Cu}$	$Surf_{Ag}$
Li^+	13.6	11.64	13.16
Na^+	14.2	10.26	11.44
K^+	14.5	7.95	8.49
Rb^+	14.6	6.97	7.23
Cs^+	14.7	4.31	4.32

Table 4. Solubility of K-based salts. Molality (mol/kg) calculated assuming the maximum concentrations feasible according to the solubility values at 20 ° C.[97] Data retrieved from Ref. [95].

Salt	*m* (mol/kg)
KBr	45
KNO_3	31.3
KOH	21.6
K_2HPO_4	8.6
K_2CO_3	8
K_2SO_4	6.9
$KHCO_3$	2.2
$KClO_4$	0.1

© 2025 The Author(s). ChemCatChem published by Wiley-VCH GmbH

centrations can overcome to solubility limit during operation and therefore generate salts. These salts can in turn block the electrode surface, even percolating through gas diffusion layers, hindering the permeation of CO_2 and poisoning the active sites. Proposed strategies to overcome this hurdle for scale-up are the use of i) catholyte-free membrane electrode assembly (MEA) as electrochemical cells (which may still suffer from cation crossover,[65] ii) salts with high solubility,[95] iii) appropriate operating conditions (*i.e.*, electrolyte temperature),[47,48] iv) pulsed electrolysis.[27,96]

6. Outlook

In this Perspective, we have initially discussed the crucial problem of carbon dioxide electroreduction, *i.e.*, CO_2 activation, and defined a classification map of transition metals, differentiating between elements which require cations to activate CO_2 and others which do not. We have then briefly summarized the concept of CCET reactions as applied to eCO_2R and H_2OR by Koper,[42] highlighting the importance of cation-induced electrostatic potential in driving CO_2 activation and water dissociation. Moving from this concept, we have then revisited our earlier DFT findings,[36,38] showing that important cation effects, such as accumulation, stabilization of CO_2, and water dissociation transition states, correlate linearly with cation-induced potential, property which can be derived from textbooks (see Table S3). Finally, we have proposed a mechanistic scheme for surface dissolution rationalizing state-of-the-art datasets *via* statistical analysis and emphasizing the role of metal cations in this process. So far, the aim of this Perspective has been to derive a simple framework to estimate the extent of cation effects in electrochemical CO_2 reduction, without the burden of long *ab initio* molecular dynamics simulations[36,38,49] or *ad hoc* multiphysics models. In this final Outlook, we mention two alternative approaches to ease the lives of computational electrochemists and one promising field of study.

6.1. Computational Cation Electrode

Beyond any doubt, the introduction of the CHE by Nørskov et al. gave a crucial boost in the field of modeling electrocatalytic reactions.[50,51] At standard conditions ($U_0 = 0.0$ V vs. SHE, bulk pH = 0, 1 bar of H_2, $T = 298.15$ K) the chemical potential μ of a proton/electron pair is equivalent to half the chemical potential of hydrogen gas, see Equation (25). This basic concept allows to correct the Gibbs free energy diagrams derived for a given electrocatalytic reaction accounting explicitly for the applied potential, provided that electron transfer steps are all assumed as proton-coupled electron transfers. For a pH different than 0, the applied potential U should be given in the reversible hydrogen through Equation 26.[50,92] k_B and T are, respectively, the Boltzmann constant and the temperature.

$$\mu_{H^+ + e^-} = \mu_{\frac{1}{2}H_2} - |e^-|U_{SHE} \tag{25}$$

$$U_{RHE} = U_{SHE} + k_B T \ln(10) \cdot pH \tag{26}$$

As mentioned, this approach has transformed the modeling field since its introduction, but its application is now falling short as in neutral to alkaline electrolyte water is the main proton source (instead of protons),[52] and some relevant electrocatalytic steps are CCTEs. Thus, the introduction of a computational cation electrode, in line with Ref. [50] is urgent. Starting from the metal cation U_0 (see Table 1),[73] we can assume that the reduction of solvated cation to the metallic state occurs at an applied potential more negative than the reduction potential, see Equation (27). Following a similar approach as for the CHE it is in principle possible to define the chemical potential of the cation/electron pair in terms of the applied electric potential and the chemical potential of the bulk metal, see Equation (28).[33] n stands for the number of water molecules in cation solvation shell. In the case of different cation concentration, it is possible to employ different extensions of the unit cell to tune cation coverage. In this direction, a positive preliminary approach was employed by Mills et al. to estimate the equilibrium potential U_0 for cation adsorption on fcc(111) facets of Ag, Au, Ni, Pd, Pt.[88]

$$Cs^+_{nH_2O} + e^- \rightarrow Cs + nH_2O \tag{27}$$

$$\mu_{Cs^+_{nH_2O}+e^-} = \mu_{Cs} + nH_2O - |e^-|(U - U_0) \tag{28}$$

6.2. Multiscale Model

An alternative approach moving away from simplicity and aiming at fully grasping the complexity of the experimental system, is the development of a self-consistent multiscale model enclosing the different length of cation processes. We have discussed above that accumulation at the surface should be properly accounted for, requiring inclusion of mass transfer effects and thus multiphysics methodologies. Besides, cations lower the activation energies of relevant steps, thus affecting reaction rates. DFT modeling allows to quantify kinetics and thermodynamics of these electrocatalytic steps, which can then be used as input in a micro-kinetic model to extract surface coverages of intermediates. Explicit solvation is a must to account for H-bond interaction of reaction intermediates or cation solvation shell, and all cation-dependent reaction steps should be explicitly considered. Finally, the cherry on top of this model would be to model as well cation-included surface reconstruction, which again depends on cation accumulation (mass transfer, multiphysics), cation-promoted formation of hydrides or carbon monoxide (surface coverage, microkinetic), stabilization of dissolution complexes (solvation effect, DFT-based molecular dynamics).

A very promising preliminary framework was devised by Lorenzutti et al.[74] Here, atomistic simulations with DFT and *ab initio* molecular dynamics were applied to estimate Gibbs free energy diagrams for hydrogen evolution and CO_2 reduction to CO on silver, assuming either proton or water as proton sources. Reaction rates were then fed into a microkinetic model to determine coverage of reaction intermediates and current

© 2025 The Author(s). ChemCatChem published by Wiley-VCH GmbH

18673899, 2025, 20, Downloaded from https://chemistry-europe.onlinelibrary.wiley.com/doi/10.1002/cctc.202500749 by Politecnico Di Torino Sist. Bibl Del Polit Di Torino, Wiley Online Library on [20/10/2025]. See the Terms and Conditions (https://onlinelibrary.wiley.com/terms-and-conditions) on Wiley Online Library for rules of use; OA articles are governed by the applicable Creative Commons License

densities. Such model was paired with a transport model including chemical equilibria in aqueous media and migration of electrolyte species. Overall, this multiscale approach allows to predict *j* vs *U* relationship purely out of simulations. Although this methodology requires further extension to more complex reaction networks (e.g., CO_2 reduction to multicarbon products) and disregard so far any evolution of the surface, we believe it is crucial milestone for further optimization.

6.3. The Potential of Organic Cations

Since its foundation, the eCO_2R field has been mainly limited to inorganic cation-based electrolytes, mainly chosen among the alkali group. Without question, $KHCO_3$ has been largely employed as the electrolyte standard in eCO_2R studies, due to its low price, although Cs^+ generally shows higher eCO_2R activity and selectivity. It is now clear that neutral pH electrolytes do not meet industrial targets of carbon conversion efficiency and long-term stability, due to the consumption of CO_2 in undesired carbonates and, consequently, formation of salts. Some efforts have been dedicated to acidic electrolytes, to limit formation of carbonates, catholyte-free membrane-electrode assembly reactors,[98] or pulsing strategies,[27,96] to prevent salt formation. None of these approaches is optimal, as acidic electrolytes and pulsed electrolysis may still be limited by competing hydrogen evolution reaction or catalyst degradation, and cation crossover occurs in MEAs.[65]

A promising approach to overcome these limitations is the use of organic cations. Pioneering studies have confirmed that eCO_2R occur employing alkali metal-free electrolytes solely composed of organic cations.[44,45] Recently, McGregor et al. have rationalized organic cation effects on eCO_2R selectivity in non-aqueous media in terms of modulation of local electric field,[46] excluding any cation–adsorbate short-term interaction characteristic of inorganic species.[36,99] Given the absence of aqueous media and molecular interactions, organic electrolytes have the potential of i) decoupling eCO_2R and HER, enabling an exclusive increase in eCO_2R selectivity; ii) opening novel optimization routes for the electrochemical Fischer–Tropsch field (currently constrained by competing HER);[16,18,100] and iii) sustaining long-term operation of industrial-scale electrolyzers. Since the environmental impact of organic electrolytes is significantly higher than inorganic counterparts, modeling studies should carry out computational screening to select promising candidates ensuring both environmental sustainability and scalability potential.

Supporting Information

The supporting information file contains:

- Figure S1, reporting the parity plot of *d*-band center of selected transition metals with and without extra electrons.
- Figure S2, reporting the parity plot of *d*-band center of selected transition metals with and without applied electric field.
- Figure S3, reporting the correlation between energy per atom on selected Cu facets and coordination number;
- Table S1, reporting the fitting parameters of the correlation of *d*-band center of selected transition metals with and without extra electrons.
- Table S2, reporting the fitting parameters of the correlation of *d*-band center of selected transition metals with and without applied electric field.
- Table S3, reporting cation properties;
- Table S4, listing the entries of the literature study on copper dissolution;
- Table S5, explaining the numerical enconding employed in the analysis;
- Table S6, listing the entries of the literature study on copper stability.

The DFT datasets generated during the current study are available at DOI: 10.19061/iochem-bd-1-379 (Ref. [101]) in the ioChem-BD database.[102]

Acknowledgments

This work has received funding from the European Union's Horizon Europe research and innovation programme under the Marie Skłodowska-Curie grant agreement no. 101104004 (SuPERCO2) and the Spanish Ministry of Science and Innovation (PID2024-157556OB-I00). We also acknowledge the support from the Barcelona Supercomputing Center (BSC-CNS) for providing generous computational resources.

Open access publishing is facilitated by Politecnico di Torino, as part of the Wiley - CRUI-CARE agreement.

Conflict of Interests

The authors declare no conflict of interest.

Data Availability Statement

The data that support the findings of this study are openly available in ioChem-BD at https://doi.org/10.19061/iochem-bd-1-379.

Keywords: Cations · Carbon dioxide fixation · Cathodic Corrosion · Surface dissolution · Water reduction

References

[1] P. Van Rysselberghe, G. J. Alkire, *J. Am. Chem. Soc.* **1944**, *66*, 1801.
[2] T. E. Teeter, P. Van Rysselberghe, *J. Chem. Phys.* **1954**, *22*, 759–760.
[3] Y. Hori, K. Kikuchi, A. Murata, S. Suzuki, *Chem. Lett.* **1986**, *15*, 897–898.
[4] Y. Hori, A. Murata, R. Takahashi, *J. Chem. Soc., Faraday Trans. 1* **1989**, *85*, 2309–2326.
[5] Y. Hori, I. Takahashi, O. Koga, N. Hoshi, *J. Phys. Chem. B* **2002**, *106*, 15–17.
[6] Y. Hori, K. Kikuchi, S. Suzuki, *Chem. Lett.* **1985**, *14*, 1695–1698.
[7] Y. Hori, A. Murata, Y. Yoshinami, *J. Chem. Soc. Faraday Trans.* **1991**, *87*, 125–128.

© 2025 The Author(s). ChemCatChem published by Wiley-VCH GmbH

18673899, 2025, 20, Downloaded from https://chemistry-europe.onlinelibrary.wiley.com/doi/10.1002/cctc.202500749 by Politecnico Di Torino Sist. Bibl Del Polit Di Torino, Wiley Online Library on [20/10/2025]. See the Terms and Conditions (https://onlinelibrary.wiley.com/terms-and-conditions) on Wiley Online Library for rules of use; OA articles are governed by the applicable Creative Commons License

[8] Y. Hori, O. Koga, H. Yamazaki, T. Matsuo, *Electrochim. Acta* **1995**, *40*, 2617–2622.
[9] O. Koga, Y. Hori, *Electrochim. Acta* **1993**, *38*, 1391–1394.
[10] Y. Tomita, Y. Hori, *Stud. Surf. Sci. Catal.* **1998**, *114*, 581–584.
[11] Y. Hori, H. Konishi, T. Futamura, A. Murata, O. Koga, H. Sakurai, K. Oguma, *Electrochim. Acta* **2005**, *50*, 5354–5369.
[12] A. Murata, Y. Hori, *Bul. Chem. Soc. Jpn.* **1991**, *64*, 123–127.
[13] A. Bagger, W. Ju, A. S. Varela, P. Strasser, J. Rossmeisl, *ChemPhysChem* **2017**, *18*, 3266–3273.
[14] A. Bagger, W. Ju, A. S. Varela, P. Strasser, J. Rossmeisl, *ACS Catal.* **2019**, *9*, 7894–7899.
[15] E. Pérez-Gallent, M. C. Figueiredo, F. Calle-Vallejo, M. T. M. Koper, *Angew. Chem. Int. Ed.* **2017**, *56*, 3621–3624.
[16] Y. Zhou, A. J. Martín, F. Dattila, S. Xi, N. López, J. Pérez-Ramírez, B. S. Yeo, *Nat. Catal.* **2022**, *5*, 545–554.
[17] R. E. Vos, M. T. M. Koper, *ACS Catal.* **2024**, *14*, 4432–4440.
[18] Y. Ou, L. Liu, R. R. Seemakurthi, F. You, H. Ma, J. Pérez-Ramírez, N. López, B. S. Yeo, *Nat. Catal.* **2025**, *8*, 714-717.
[19] T. J. Hersbach, I. T. McCrum, D. Anastasiadou, R. Wever, F. Calle-Vallejo, M. T. M. Koper, *ACS Appl. Mater. Interfaces* **2018**, *10*, 39363–39379.
[20] T. J. P. Hersbach, M. T. M. Koper, *Curr. Opin. Electrochem.* **2021**, *26*, 100653.
[21] T. J. P. Hersbach, A. T. Garcia-Esparza, S. Hanselman, O. A. Paredes Mellone, T. Hoogenboom, I. T. McCrum, D. Anastasiadou, J. T. Feaster, T. F. Jaramillo, J. Vinson, T. Kroll, A. C. Garcia, P. Krtil, D. Sokaras, M. T. M. Koper, *Nat. Mater.* **2025**, *24*, 574–580.
[22] J. Huang, N. Hörmann, E. Oveisi, A. Loiudice, G. L. De Gregorio, O. Andreussi, N. Marzari, R. Buonsanti, *Nat. Commun.* **2018**, *9*, 3117.
[23] J. Vavra, T.-H. Shen, D. Stoian, V. Tileli, R. Buonsanti, *Angew. Chem. Int. Ed.* **2021**, *60*, 1347–1354.
[24] R. Amirbeigiarab, J. Tian, A. Herzog, C. Qiu, A. Bergmann, B. R. Cuenya, O. M. Magnussen, *Nat. Catal.* **2023**, *6*, 837–846.
[25] J. Vavra, G. P. Ramona, F. Dattila, A. Kormányos, T. Priamushko, P. P. Albertini, A. Loiudice, S. Cherevko, N. López, R. Buonsanti, *Nat. Catal.* **2024**, *7*, 89–97.
[26] S. Liu, Y. Li, D. Wang, S. Xi, H. Xu, Y. Wang, X. Li, W. Zang, W. Liu, M. Su, K. Yan, A. C. Nielander, A. B. Wong, J. Lu, T. F. Jaramillo, L. Wang, P. Canepa, Q. He, *Nat. Commun.* **2024**, *15*, 5080.
[27] Z. Li, L. Wang, L. Sun, W. Yang, *J. Am. Chem. Soc.* **2024**, *146*, 23901–23908.
[28] S. Ringe, E. L. Clark, J. Resasco, A. Walton, B. Seger, A. T. Bell, K. Chan, *Energy Environ. Sci.* **2019**, *12*, 3001–3014.
[29] M. R. Singh, Y. Kwon, Y. Lum, J. W. Ager III, A. T. Bell, *J. Am. Chem. Soc.* **2016**, *138*, 13006–13012.
[30] O. Ayemoba, A. Cuesta, *ACS Appl. Mater. Interfaces* **2017**, *9*, 27377–27382.
[31] F. Zhang, A. C. Co, *Angew. Chem. Int. Ed.* **2020**, *59*, 1674–1681.
[32] L. D. Chen, M. Urushihara, K. Chan, J. K. Nørskov, *ACS Catal.* **2016**, *6*, 7133–7139.
[33] J. Resasco, L. D. Chen, E. Clark, C. Tsai, C. Hahn, T. F. Jaramillo, K. Chan, A. T. Bell, *J. Am. Chem. Soc.* **2017**, *139*, 11277–11287.
[34] M. M. Waegele, C. M. Gunathunge, J. Li, X. Li, *J. Chem. Phys.* **2019**, *151*, 160902.
[35] S. Ringe, *Curr. Opin. Electrochem.* **2023**, *39*, 101268.
[36] M. C. O. Monteiro, F. Dattila, B. Hagedoorn, R. García-Muelas, N. López, M. T. M. Koper, *Nat. Catal.* **2021**, *4*, 654–662.
[37] S.-J. Shin, H. Choi, S. Ringe, D. H. Won, H.-S. Oh, D. H. Kim, T. Lee, D.-H. Nam, H. Kim, C. H. Choi, *Nat. Commun.* **2022**, *13*, 5482.
[38] M. C. O. Monteiro, F. Dattila, N. López, M. T. M. Koper, *J. Am. Chem. Soc.* **2022**, *144*, 1589–1602.
[39] J. T. Bender, A. S. Petersen, F. C. Østergaard, M. A. Wood, S. M. J. Heffernan, D. J. Milliron, J. Rossmeisl, J. Resasco, *ACS Energy Lett.* **2023**, *8*, 657–665.
[40] S. Vijay, W. Ju, S. Brückner, S.-C. Tsang, P. Strasser, K. Chan, *Nat. Catal.* **2021**, *4*, 1024–1031.
[41] C. Ye, F. Dattila, X. Chen, N. López, M. T. M. Koper, *J. Am. Chem. Soc.* **2023**, *145*, 19601–19610.
[42] M. T. M. Koper, *J. Solid State Electrochem.* **2024**, *28*, 1–6.
[43] H. Kim, M. M. Kim, J. Cho, S. Lee, D. H. Kim, S.-J. Shin, T. Utsunomiya, W. A. Goddard III, Y. Katayama, H. Kim, C. H. Choi, *J. Am. Chem. Soc.* **2025**, *147*, 4667–4674.
[44] S. Weng, W. L. Toh, Y. Surendranath, *J. Am. Chem. Soc.* **2023**, *145*, 16787–16795.
[45] H.-G. Qin, Y.-F. Du, Y.-Y. Bai, F.-Z. Li, X. Yue, H. Wang, J.-Z. Peng, J. Gu, *Nat. Commun.* **2023**, *14*, 5640.
[46] J.-M. McGregor, J. T. Bender, A. S. Petersen, L. Cañada, J. Rossmeisl, J. F. Brennecke, J. Resasco, *Nat. Catal.* **2025**, *8*, 79–91.
[47] J. Biemolt, J. Singh, G. Prats Vergel, H. M. Pelzer, T. Burdyny, *ACS Energy Lett.* **2025**, *10*, 807–814.
[48] H. M. Pelzer, N. Kolobov, D. A. Vermaas, T. Burdyny, *Nat. Energy* **2025**, *10*, 549–556.
[49] F. Dattila, M. C. O. Monteiro, M. T. M. Koper, N. López, *Nat. Catal.* **2022**, *5*, 979–981.
[50] J. K. Nørskov, J. Rossmeisl, A. Logadottir, L. Lindqvist, J. R. Kitchin, T. Bligaard, H. Jónsson, *J. Phys. Chem. B* **2004**, *108*, 17886–17892.
[51] A. A. Peterson, F. Abild-Pedersen, F. Studt, J. Rossmeisl, J. K. Nørskov, *Energy Environ. Sci.* **2010**, *3*, 1311–1315.
[52] Y. Y. Birdja, E. Pérez-Gallent, M. C. Figueiredo, A. J. Göttle, F. Calle-Vallejo, M. T. M. Koper, *Nat. Energy* **2019**, *4*, 732–745.
[53] H. A. Schwarz, R. W. Dodson, *J. Phys. Chem.* **1989**, *93*, 409–414.
[54] R. García-Muelas, F. Dattila, T. Shinagawa, A. J. Martín, J. Pérez-Ramírez, N. López, *J. Phys. Chem. Lett.* **2018**, *9*, 7153–7159.
[55] Creative Commons Attribution 4.0 International License, http://creativecommons.org/licenses/by/4.0/, online; accessed 24 April 2025.
[56] J. P. Perdew, K. Burke, M. Ernzerhof, *Phys. Rev. Lett.* **1996**, *77*, 3865–3868.
[57] S. Grimme, *J. Comput. Chem.* **2006**, *27*, 1787–1799.
[58] T. Bučko, J. Hafner, S. Lebegue, J. G. Angyán, *J. Phys. Chem. A* **2010**, *114*, 11814–11824.
[59] N. Almora-Barrios, G. Carchini, P. Błoński, N. López, *J. Chem. Theory Comput.* **2014**, *10*, 5002–5009.
[60] P. E. Blöchl, *Phys. Rev. B* **1994**, *50*, 17953–17979.
[61] G. Kresse, D. Joubert, *Phys. Rev. B* **1999**, *59*, 1758–1775.
[62] H. J. Monkhorst, J. D. Pack, *Phys. Rev. B* **1976**, *13*, 5188–5192.
[63] L. Vitos, A. Ruban, H. Skriver, J. Kollár, *Surf. Sci.* **1998**, *411*, 186–202.
[64] G. Makov, M. C. Payne, *Phys. Rev. B* **1995**, *51*, 4014–4022.
[65] G. A. El-Nagar, F. Haun, S. Gupta, S. Stojkovikj, M. T. Mayer, *Nat. Commun.* **2023**, *14*, 2062.
[66] Y. Morimoto, H. Kotani, J. Park, Y.-M. Lee, W. Nam, S. Fukuzumi, *J. Am. Chem. Soc.* **2011**, *133*, 403–405.
[67] S. Fukuzumi, K. Ohkubo, Y. Morimoto, *Phys. Chem. Chem. Phys.* **2012**, 8472–8484.
[68] M. T. M. Koper, G. A. Voth, *Chem. Phys. Lett.* **1998**, *282*, 100–106.
[69] D. Bohra, J. H. Chaudhry, T. Burdyny, E. A. Pidko, W. A. Smith, *Energy Environ. Sci.* **2019**, *12*, 3380–3389.
[70] T. H. Phan, K. Banjac, F. P. Cometto, F. Dattila, R. García-Muelas, S. J. Raaijman, C. Ye, M. T. M. Koper, M. Lingenfelder, *Nano Lett.* **2021**, *21*, 2059–2065.
[71] A. Goyal, M. T. M. Koper, *Angew. Chem. Int. Ed.* **2021**, *60*, 13452–13462.
[72] Y. Marcus, *Chem. Rev.* **1988**, *88*, 1475–1498.
[73] W. Haynes, D. Lide, *Handbook of Chemistry and Physics*, 92nd ed., CRC Press, Boca Raton, FL, **2011**.
[74] F. Lorenzutti, R. R. Seemakurthi, E. F. Johnson, S. Morandi, P. Nikačević, N. López, S. Haussener, *Nat. Catal.* **2025**, https://doi.org/10.1038/s41929-025-01399-2.
[75] L. Bellarosa, R. García-Muelas, G. Revilla-López, N. López, *ACS Cent. Sci.* **2016**, *2*, 109–116.
[76] F. Dattila, Cation effect CO_2 reduction, *ioChem-BD*, https://doi.org/10.19061/iochem-bd-1-194 , online; accessed 24 April 2025.
[77] F. Dattila, Multivalent cation effect CO_2 H_2O reduction, *ioChem-BD*, https://doi.org/10.19061/iochem-bd-1-213 , online; accessed 24 April 2025.
[78] P. J. Feibelman, *Phys. Rev. B* **2001**, *64*, 125403.
[79] J. Gu, S. Liu, W. Ni, W. Ren, S. Haussener, X. Hu, *Nat. Catal.* **2022**, *5*, 268–276.
[80] F. Dattila, Candidate Materials COR, *ioChem-BD*, https://doi.org/10.19061/iochem-bd-1-245, online; accessed 24 April 2025.
[81] I. T. McCrum, M. T. M. Koper, *Nat. Energy* **2020**, *5*, 1–9.
[82] A. Goyal, G. Marcandalli, V. A. Mints, M. T. M. Koper, *J. Am. Chem. Soc.* **2020**, *142*, 4154–4161.
[83] M. C. O. Monteiro, A. Goyal, P. Moerland, M. T. M. Koper, *ACS Catal.* **2021**, *11*, 14328–14335.
[84] I. T. McCrum, C. J. Bondue, M. T. M. Koper, *J. Phys. Chem. Lett.* **2019**, *10*, 6842–6849.

© 2025 The Author(s). ChemCatChem published by Wiley-VCH GmbH

18673899, 2025, 20, Downloaded from https://chemistry-europe.onlinelibrary.wiley.com/doi/10.1002/cctc.202500749 by Politecnico Di Torino Sist. Bibl Del Polit Di Torino, Wiley Online Library on [20/10/2025]. See the Terms and Conditions (https://onlinelibrary.wiley.com/terms-and-conditions) on Wiley Online Library for rules of use; OA articles are governed by the applicable Creative Commons License

[85] F. D. Speck, A. Zagalskaya, V. Alexandrov, S. Cherevko, *Angew. Chem. Int. Ed.* **2021**, *60*, 13343–13349.
[86] F. Haber, *Zeitschrift für anorganische Chemie* **1898**, *16*, 438–449.
[87] F. Haber, *Trans. Am. Electrochem. Soc.* **1902**, *2*, 189–196.
[88] J. N. Mills, I. T. McCrum, M. J. Janik, *Phys. Chem. Chem. Phys.* **2014**, *16*, 13699.
[89] I. T. McCrum, M. J. Janik, *J. Phys. Chem.* **2016**, *120*, 457–471.
[90] H. M. Polatoglou, M. Methfessel, M. Scheffler, *Phys. Rev. B* **1993**, *48*, 1877–1883.
[91] S. J. Raaijman, M. P. Schellekens, P. J. Corbett, M. T. M. Koper, *Angew. Chem. Int. Ed.* **2021**, *60*, 21732–21736.
[92] A. J. Bard, L. R. Faulkner, *Electrochemical Methods: Fundamentals and Applications*, 2nd ed, John Wiley & Sons, Inc., Hoboken, NJ **2001**.
[93] M. R. Singh, E. L. Clark, A. T. Bell, *Phys. Chem. Chem. Phys.* **2015**, *17*, 18924–18936.
[94] A. S. Malkani, J. Anibal, B. Xu, *ACS Catal.* **2020**, *10*, 14871–14876.
[95] M. C. O. Monteiro, M. F. Philips, K. J. P. Schouten, M. T. M. Koper, *Nat. Commun.* **2021**, *12*, 4943.
[96] H. Ma, E. Ibáñez-Alé, R. Ganganahalli, J. Pérez-Ramírez, N. López, B. S. Yeo, *J. Am. Chem. Soc.* **2023**, *145*, 24707–24716.
[97] C. M. Hansen, *Hansen Solubility Parameters: A User's Handbook*, CRC Press, Boca Raton, FL **2007**.
[98] A. Ozden, F. P. García de Arquer, J. E. Huang, J. Wicks, J. Sisler, R. K. Miao, C. P. O'Brien, G. Lee, X. Wang, A. H. Ip, E. H. Sargent, D. Sinton, *Nat. Sustain.* **2022**, *5*, 563–573.
[99] M. J. Janik, *Nature Catalysis* **2025**, *8*, 9–10.
[100] P. Preikschas, J. Zhang, R. R. Seemakurthi, Z. Lian, A. J. Martín, S. Xi, F. Krumeich, H. Ma, Y. Zhou, N. López, B. S. Yeo, J. Pérez-Ramírez, *Adv. Energy Mater.* **2024**, *14*, 2401447.
[101] F. Dattila, Cation Potential, *ioChem-BD*, https://doi.org/10.19061/iochem-bd-1-379, online; accessed 24 April 2025.
[102] M. Álvarez-Moreno, C. de Graaf, N. López, F. Maseras, J. Poblet, C. Bo, *J. Chem. Inf. Model.* **2015**, *55*, 95–103.

Manuscript received: April 24, 2025
Revised manuscript received: July 25, 2025
Accepted manuscript online: July 31, 2025
Version of record online: September 14, 2025

© 2025 The Author(s). ChemCatChem published by Wiley-VCH GmbH

18673899, 2025, 20, Downloaded from https://chemistry-europe.onlinelibrary.wiley.com/doi/10.1002/cctc.202500749 by Politecnico Di Torino Sist. Bibl Del Polit Di Torino, Wiley Online Library on [20/10/2025]. See the Terms and Conditions (https://onlinelibrary.wiley.com/terms-and-conditions) on Wiley Online Library for rules of use; OA articles are governed by the applicable Creative Commons License